Performance Analysis of Wells Turbine Blades Using the Entropy Generation Minimization Method

Ahmed S. Shehata[1, 3*], Khalid M. Saqr[2], Qing Xiao [1], Mohamed F. Shehadeh [3], Alexander Day[1]

1) *Department of Naval Architecture, Ocean and Marine Engineering, University of Strathclyde, Glasgow G4 0LZ, U.K*
2) *Mechanical Engineering Department, College of Engineering and Technology Arab Academy for Science Technology and Maritime Transport, P.O. 1029 AbuKir, Alexandria, EGYPT*
3) *Marine Engineering Department, College of Engineering and Technology Arab Academy for Science Technology and Maritime Transport, P.O. 1029 AbuQir, Alexandria, EGYPT*
* Corresponding Author: Ahmed S. Shehata, E-mail address: ahmed.mohamed-ahmed-shehata@strath.ac.uk

ABSTRACT

Wells turbine concept depends on utilizing the oscillating air column generated over marine waves to drive a turbine. As a matter of fact, previous researches on the performance analysis of such turbine were based on the first law of thermodynamics only. Nonetheless, the actual useful energy loss cannot be completely justified by the first law because it does not distinguish between the quantity and the quality of energy. Therefore, the present work investigates the second law efficiency and entropy generation characteristics around different blades that are used in Wells turbine under oscillating flow conditions. The work is performed by using time-dependent CFD models of different NACA airfoils under sinusoidal flow boundary conditions. Numerical investigations are carried out for the incompressible viscous flow around the blades to obtain the entropy generation due to viscous dissipation. It is found that the value of second law efficiency of the NACA0015 airfoil blade is higher by approximately 1.5% than the second law efficiency of the NACA0012, NACA0020 and NACA0021 airfoils. Furthermore, it is found that the angle of attack radically affects the second law efficiency and such effect is quantified for NACA0015 for angle of attack ranging from -15º to 25º.

Keywords: Wells turbine; entropy generation; NACA airfoils; sinusoidal wave; CFD.

36 **NOMENCLATURE**

A	Cross-sectional area of cylinder (m^2)
B	Cord of cylinder (cm)
f	cycle frequency (Hz)
F_D	In-line force acting on cylinder per unit length (gf)
KE	Kinetic Energy (W/K)
L	Blade Chord (m)
p	Pressure field (Pa)
S_{gen}	local entropy generation rate (W/m^2K)
S_G	Global entropy generation rate (W/K)
S_{ij}	Mean strain rate
S_t	Thermal entropy generation rate (W/m^2K)
S_V	Viscous entropy generation rate (W/m^2K)
T_o	Reservoir temperature (K)
$\bar{u}_i$	Reynolds Averaged velocity component in i direction (m/s)
V	Instantaneous Velocity (m/s)
V_a	highest speed of axial direction (m/s)
V_o	Initial velocity for computation (m/s)
W_{rev}	Reversible work
μ	Viscosity (Kg/ms)
μ_t	Turbulent viscosity
ρ	Density (Kg/m^3)
$\sigma_\epsilon, \sigma_k$	The turbulent Prandtl numbers for κ and ε respectively
$\left(-\overline{\rho u'_i u'_j}\right)$	Reynolds stress tensor

37

38

1.   INTRODUCTION

The major challenge facing oscillating water column systems is to find efficient and economical means of converting oscillating flow energy to unidirectional rotary motion, for driving electrical generators. A novel resolution for such challenge is the Wells turbine [1-4], see figure 1(a, b) due to its simple and efficient operation. The Wells turbine has already been applied in practice to gain energy from marine waves. In the past two decades, experimental research of Wells turbine has mainly focused on improving the turbine performance with emphasis on the overall operational characteristics. The airfoils sections that are used in Wells turbine have been extensively investigated in aeronautical applications. However, the operating conditions in Wells turbine are completely different from such of the aeronautical applications. In Wells turbine, the rotor contains multiple blades, which are confined by a shroud aiming at harnessing the flow momentum to drive the rotor with the maximum torque. The flow physics in such situations are still having several issues to investigate; besides, the dynamical complexity resulting from an oscillating water column driven by random irregular marine waves.

Second law analysis of energy conversion systems has become an important tool for optimization and development during the past decade. In Fact, the second law of thermodynamics is more reliable than the first law of thermodynamics analysis due to the limitation of the first law efficiency in a heat transfer engineering systems as well as heat transfer, mass transfer, viscous dissipation, etc. Moreover, the second law can be used as the sources of entropy generation [5, 6].Consequently, This work utilizes time-dependent numerical models of different NACA four-digit series blade profile under oscillating flow conditions. Numerical investigations are carried out for the flow around Wells turbine blades using sinusoidal wave boundary conditions to perform as realistic characterization as possible of the flow field upstream and downstream of the turbine during the passage of the wave. The Gouy–Stodola theorem [7] has been used to compute the second law efficiency from the results of the numerical simulations. This theorem postulates the difference between reversible and actual works in any thermodynamic system which is the entropy generation in such system, as discussed later in section 4. Such theorem is the foundation for the entropy generation

71 minimization method proposed by Bejan [8] to optimize finite size thermodynamic
72 systems.

73 A thorough literature survey has revealed that the second law analysis of the
74 oscillating flow around wells turbine has not been conducted before. However, this
75 section briefly reviews the most relevant studies to accentuate the scope of the present
76 work. In a number of previous studies, it is concluded that the delay of stall onset
77 contributes in improving Wells turbine performance. This delay can be achieved by
78 setting guide vanes on the hub near the rotor[9].

79 As far as the running and starting characteristics of the Wells turbine are
80 concerned, Wells turbine with 3D guide vanes are superior to those with 2D guide vanes
81 or without guide vanes[10, 11]. Furthermore, the presence of end plates is investigated
82 experimentally and numerically by [12, 13] where they conclude that the Wells turbine
83 with end plates is superior to those of the original Wells turbine(which was investigated
84 also in this work) because the peak efficiency and the stall margin increases by
85 approximately 4% and its characteristics are dependent on the size and position of end
86 plate.

87

88 Three dimensional numerical simulations are performed by Thakker et al [14] in
89 order to analyze the performance of a Wells turbine with CA9 blade profile, a maximum
90 efficiency of 70% is obtained. Moreover, Kim et al [15] uses numerical simulation to
91 study the effect of the blade sweep on the performance of a Wells turbine using either
92 NACA0020 or CA9 blade profiles. They were found that the performance of the Wells
93 turbines with NACA0020 and the CA9 blades are influenced by the blade sweep. As the
94 optimum rotor shape for a NACA0020 blade, a blade sweep ratio 35% is identified to
95 deliver the optimum performance. In general, the overall turbine performance for the
96 NACA0020 is better than such of the CA9, Also, Takao et al [16], presents
97 experimentally the suitable choice the sweep ratio of 0.35 for the cases of CA9 and
98 HSIM 15-262123-1576. In another study [17], the characteristics of a Wells turbine
99 with NACA0021 constant chord blades are investigated. They find from the numerical
100 results that the wakes behind the turbine blades merge rigorously in the portion of radius
101 ratio from 0.45 to 1.0, which leads the turbine to stall.

102

103   One and two stage Wells turbines involving symmetric airfoils and Non-
104   Symmetric airfoils are investigated by Mohamed [18, 19]. Numerical optimization
105   procedure has been carried out to optimize the performance of the turbine as a function
106   of the non-dimensional gap between the two rotors. It is leading to an optimal value of
107   the non-dimensional gap (The distance between the two stages / the blade chord) near
108   0.85 when considering the operating range. Moreover, the Evolutionary Algorithms are
109   used to estimate the optimum shape with an increase of efficiency (by 2.1%) and of
110   tangential force coefficient (by 6%), compared to the standard NACA 2421, as well as
111   the one-stage the optimum shape with an increase of efficiency (by 1%) and of
112   tangential force coefficient (by 11.3%), compared to the standard NACA 0021.

113

114   On the other hand, the hysteretic characteristics of monoplane and biplane have
115   been studied in a number of studies [20-26]. The objective of such works is mainly to
116   investigate the aerodynamic losses of Wells turbine. It is found that for the biplane, the
117   hysteretic behavior is similar to that of the monoplane at lower angles of attack, but the
118   hysteretic loop similar to the dynamic stall is observed at higher angles of attack.
119   Exergy analysis is performed using the numerical simulation for steady state biplane
120   Wells turbines [27] where the upstream rotor has a design point second law efficiency
121   of 82.3% although the downstream rotor second law efficiency equals 60.7%.

122

123   Most of the researchers who have investigated the performance of different
124   airfoils design and different operational condition have analyzed the problem using only
125   the parameter of first law of thermodynamic that lead to several contradicting
126   conclusions that can be observed, for example, in [28].This shows that the use of two
127   twin rotors rotating in the opposite direction to each other is an efficient means of
128   recovering the swirl kinetic energy without the use of guide vanes. On quite the
129   opposite, a contra-rotating W-T which is investigated in [29], it is found to have a
130   lower efficiency than a biplane or monoplane W-T with guide vanes. Another example,
131   we can observe this contradiction also in the comparison between the performances of
132   the Wells turbines in four different kinds of blade profile (NACA0020; NACA0015;
133   CA9; and HSIM 15-262123-1576). Which, the blade profile of (NACA0020) have the
134   best performance according to the result of [16, 30], but, according to the result of [31]

135 the blade profile of (NACA0015) achieve best result. Finally, the rotor geometry

136 preferred was the blade profile of (CA9) according to the result of [32, 33].

137 It is essential to look at the second law of thermodynamic to form a deeper

138 understanding, since it has shown very promising result in many applications, like wind

139 turbine in [34-38], Radial Compressor Stage [39], pipe flow [40], thermal power plants

140 [6], and Rotating disk [5].

141

142 The objective of the present work is essentially to investigate the entropy

143 generation, due to viscous dissipation, around Wells turbine airfoils in two-

144 dimensional unsteady flow configurations. The research aims to use the entropy

145 generation due to viscous dissipation around a Wells turbine blade as very

146 sensitive judged parameter on the turbine performance for any change in terms

147 of the operating condition (the flow Reynolds number up to 2.4×10^5 and the

148 airfoil angle of attack from -15 to 25 degree), the blade design (four different

149 airfoils) and flow direction (sinusoidal wave with compression and suction

150 cycle). This work is limited to four airfoils namely NACA0012, NACA0015,

151 NACA0020 and NACA0021. These airfoils are common to use in Wells turbine

152 applications.

153

154 **2.   MATHMEATICAL MODEL AND NUMERICAL APPROACH**

155

156 The mathematical model consists of the governing equations of turbulent

157 incompressible unsteady flow in two-dimensional generalized coordinates, which can be

158 written in vector notations as[41]:

159 Continuity: $\dfrac{\partial}{\partial t}+\dfrac{\partial}{\partial x_i}\left(\bar{u}_i\right)=0$ (1)

160 RANS: $\rho\dfrac{\partial \bar{u}_i}{\partial t}+\dfrac{\partial}{\partial x_i}\left(\rho\bar{u}_i\bar{u}_j\right)=-\dfrac{\partial p}{\partial x_j}+\dfrac{\partial}{\partial x_j}\left[\mu\left(\dfrac{\partial \bar{u}_i}{\partial x_j}+\dfrac{\partial \bar{u}_j}{\partial x_i}-\dfrac{2}{3}\delta_{ij}\dfrac{\partial \bar{u}_j}{\partial x_i}\right)\right]+\dfrac{\partial}{\partial x_j}\left(-\overline{\rho u_i'u_j'}\right)$

161 (2)

162 and turbulent flow is modeled using the Realizable k-e model, Transport equation of

163 turbulent kinetic energy (k)

$$\frac{\partial}{\partial t}(\rho k)+\rho\frac{\partial}{\partial x_i}(U_i k)=\frac{\partial}{\partial x_j}\left[\left(\mu+\frac{\mu_T}{\sigma_k}\right)\frac{\partial}{\partial x_j}k\right]_6^{164}+\mu_T S^2-\rho\,\varepsilon$$

165   (3)

166 Specific dissipation rate equation is:

167

$$\frac{\partial}{\partial t}(\rho\varepsilon) + \rho\frac{\partial}{\partial x_i}(U_i\varepsilon) = \frac{\partial}{\partial x_j}\left[\left(\mu + \frac{\mu_T}{\sigma_\varepsilon}\right)\frac{\partial}{\partial x_j}\varepsilon\right] + C_1\rho S_\varepsilon - C_2\rho\frac{\varepsilon^2}{k + \sqrt{v\varepsilon}}$$

169   (4)

170

171 Where

172 $$C_1 = max\left(0.43, \frac{\eta}{\eta + 5}\right), \qquad C_2 = 1.9$$

$$C_\mu = \frac{1}{A_0 + A_s U^* \frac{k}{\varepsilon}}$$

                                                (5)

175 Where

$$A_0 = 4.0, U^* = \sqrt{S_{ij}S_{ij} + \Omega_{ij}\Omega_{ij}}, A_s = \sqrt{6}\cos\left(\frac{1}{3}arccos\left(\sqrt{6}W\right)\right), W = \frac{\sqrt{8}\, S_{ij}S_{jk}S_{ki}}{S^3}$$

176

177

178 and the vorticity tensor $\quad \Omega_{ij} = \frac{1}{2}\left(\frac{\partial\overline{u}_i}{\partial x_j} - \frac{\partial\overline{u}_j}{\partial x_i}\right)$

179

180 where $\overline{u}$ is the Reynolds averaged velocity vector. The present study adopts one and

181 two-equation turbulence models to close the Reynolds stress term $\left(-\overline{\rho u_i' u_j'}\right)$ of the

182 RANS equation [42] as shown in the following section. The transport equations of such

183 models can be found in turbulence modeling texts such as [43].The second law of

184 thermodynamic defines the net-work transfer rate $\dot{W}$ as [8]:

185 $\dot{W} = W_{rev} - T_o S_{gen}$ (6)

186

187   It is possible to express the irreversible entropy generation in terms of the

188 derivatives of local flow quantities in the absence of phase changes and chemical

189 reactions. The two dissipative mechanisms in viscous flow are the strain-originated

190 dissipation and the thermal dissipation Which correspond to a viscous and a thermal

191 entropy generation respectively [39]. Thus, it can be written,

192 $S_{gen} = S_V + S_{th}$ (7)

193   In incompressible isothermal flow, such as the case in hand, the thermal

194   dissipation term vanishes. The local viscous irreversibilities therefore can be expressed

195   as:

196     $$S_V = \frac{\mu}{T_o} \phi \tag{8}$$

197   where ϕ is the viscous dissipation term, that is expressed in two dimensional Cartesian

198   coordinates as [39]:

199     $$\phi = 2 \left[\left(\frac{\partial u}{\partial x} \right)^2 + \left(\frac{\partial v}{\partial y} \right)^2 \right] + \left(\frac{\partial u}{\partial y} + \frac{\partial v}{\partial x} \right)^2 \tag{9}$$

200   and the global entropy generation rate is hence expressed as:

201     $$S_G = \iint_{xy} S_V \, dy \, dx \tag{10}$$

202   and finely the second law efficiency is defined as :

203     $$\eta_S = \frac{KE}{KE + S_G} \tag{11}$$

204   where $KE = \frac{1}{2} V^2$ $\tag{12}$

205   but the efficiency in first law of thermodynamics (η_f) is defined as:

206

        $$\eta_f = \frac{Net\ Output}{Total\ work\ Input} \tag{13}$$

207

208   **2.1   Numerical Model Details**

209   The computational domain is discretized to Cartesian structured finite

210   volume cells using GAMBIT code. Drichlet boundary conditions are applied on

211   the domain for the solution of momentum and continuity equations. The

212   application of such boundary condition types [21, 44-46] matches the Green-

213   Gauss cell based evaluation method for the gradient terms used in the solver

214   (ANSYS FLUENT). Numerous tests accounting for different interpolation

215   schemes used to compute cell face values of the flow field variables, the

216   variables of governing equation which are velocity and pressure, as well as

217   convergence tests have been undertaken. The second order upwind interpolation

218   scheme is used in this work because it yields results which are approximately

8

similar to such yielded by third order MUSCL scheme in the present situation. It is also found that the solution reaches convergence when the scaled residuals approaches 1×10^{-5}. At such limit, the flow field variables holds constant values with the application of consecutive iterations. Figure (2); show the dimensions of whole computational domain and location of airfoil. Figure (3) show the grid distribution near the wall of the airfoil.

The axial flow of Wells Turbine is modeled as a sinusoidal wave in this simulation. Therefore, Inlet boundary conditions are set to change as time. In order to apply the inlet boundary condition, inlet velocity with periodic function (see figure 4) is generated as follows.

$$V = V_o + V_a (\sin 2 \pi f t) \qquad\qquad (14)$$

where t is time period 6.7 seconds are set as one period in this simulation considering to the literature survey [22, 23, 33]. Time step is set as 0.00009 second in order to satisfy CFL (Courant Friedrichs Lewy) [47] condition equal to 1. the sinusoidal wave condition create various Reynolds number up to 2.4×10^5 and this maximum value which is taken from many references such as [13, 18, 20-23, 25, 48, 49]. Regarding the angle of attack, it covers wide range of angles of attack in both directions (positive and negative) but it doesn't need more than this value because the stall condition [50].

2.2 Numerical Model Validation

In order to ensure that the numerical model is free from numerical errors, several grids are tested to estimate the number of grid cells required to establish a grid-independent test. Table 1 shows the specifications of different grids used in such test. Figure 5 shows the pressure coefficient (C_p) distribution on the upper and lower surfaces of the airfoil as computed by the four grids. Grid C and D have the same result, but the latter one required less time. So, Grid C is chosen to conduct the analysis presented hereafter.

Many turbulence models are used to model the oscillating flow around the object in order to determine the model which gives the best agreement with

9

251	experimental data adopted from [51]. The best result for S-A, $k - \omega$ SST and
252	the Realizable $k - \varepsilon$ model but the latter one required less time [52]. As For the
253	near-wall treatment in both K-epsilon and S-A models have used the log law of
254	the wall but for k-omega models have used y plus less than one. This
255	experimental data for unsteady forces acting on a square cylinder in oscillating
256	flow with nonzero mean velocity are measured [51] where the oscillating air
257	flows are generated by a unique AC servomotor wind tunnel. The generated
258	velocity histories are almost exact sinusoidal waves. The measured unsteady F_D
259	is computed from the Morison equation for the in-line force acting on the
260	cylinder per unit length:

261

$$F_D = \frac{1}{2} \rho B C_D |U| U + \rho A \widetilde{C}_D \dot{U} \qquad (15)$$

262	where $\dot{U} = dU/dt$ and the non-dimensional coefficient $\widetilde{C}_D$ is the inertia
263	coefficient of the unsteady in-line force. This non-dimensional coefficient is
264	evaluated depend on [53, 54].
265	This data is the most experimental data that have available information for the
266	sinusoidal flow condition to validate our work; therefore, it is adopted in the
267	following simulation cases. Figure 6 (a), (b) show an excellent agreement
268	between measured drag force from reference and calculated drag force from
269	CFD at two different frequency.

270

271   **3.**   **RESULTS AND DISCUSSION**

272   **3.1 Evaluation of the second law efficiency of different NACA airfoils**

273	The numerical simulations are used to obtain local entropy viscosity
274	predictions of the different airfoil sections. Figure 7(a) and (b) highlight the
275	entropy behavior when a flow is accelerating in compression and suction cycle.
276	Consequently, the entropy generation ratio various with the Reynolds number at
277	certain angle of attack equal to 2 degree. The change of Reynolds number values
278	is due to using sinusoidal wave boundary conditions. At low values of Reynolds
279	number the stall condition occur at small value of angle of attack[50]. Hence, 2
280	degree angle of attack is chosen to avoid the stall condition.

281   The Reynolds number is calculated from equation (14). Otherwise, the value

282   of Reynolds number in this study can be controlled by the value of velocity while

283   keeping the other parameters constant.

284    $$\text{Re} = \frac{VL\rho}{\mu} \qquad\qquad (16)$$

285   The Reynolds number has radical effect on the entropy generation. This is

286   obvious in the accelerating flow in compression and suction cycle in Figure 7 (a,

287   b), where Reynolds number increase from 6×10^4 to 1.2×10^5. As a result, the global

288   entropy generation rate (i.e. integral) has increased correspondingly for more than

289   two folds of all airfoils. However, when Reynolds number has increased further to

290   1.7×10^5 (2×10^5 for NACA0012 at compression cycle) the global entropy

291   generation rate exhibited unintuitive values ranging from 50% less to 40% lower

292   than the corresponding value at Reynolds number equal to 1.2×10^5 for all airfoils.

293   The reason behind such phenomena can be attributed to the nonlinear complexity

294   of the viscous dissipation term (equation 9) where both the square of mean rate of

295   strain and velocity divergence contributes to the local viscous irreversibilities.

296   This phenomenon suggests that possible existence of critical Reynolds number at

297   which viscous irreversibility takes minimum values. At high Reynolds number

298   (greater than 2×10^5) the change in velocity value, see equation 14, is smaller than

299   low Reynolds number. Where, at 120000 Reynolds number the velocity equal to

300   17.5 m/s, then it increases to 24.8 m/s at 170000 Reynolds number (41%increase

301   rate). After that, it reaches to 200000 Reynolds number with velocity equal to 30.3

302   m/s (22%increase rate). On the other hand, at high Reynolds number (230000) the

303   velocity equal to 33.8 m/s (10%increase rate). Then, at 240000 Reynolds number

304   the velocity reach to maximum value equal to 35.04 m/s (3%increase rate), see

305   Figure 4. This leads to smaller change in flow field and entropy generation. The

306   last one was dependent on velocity analysis.

307

308   However, in figure 8 (a, b) for decelerating flow in compression and suction

309   cycle when Reynolds number, in Figure (8, a), is decreased further to 1.2×10^5 the

310   global entropy generation rate exhibited unintuitive values ranging from 94%

311   (NACA0021, NACA0020) less to 59% (NACA0015) and 15% for (NACA0012)

312   higher than the corresponding value at Reynolds number equal to 1.7×10^5. For

313   decelerating flow in suction cycle the global entropy generation rate, at Reynolds

314   number equal to 1.2×10^5, exhibited unintuitive values ranging from 135%

315   (NACA0012) less to 83% (NACA0020) and 68% (NACA0021, NACA0015)

316   which is higher than the corresponding value at Reynolds number equal to

317   1.7×10^5. Then, when Reynolds number is decreased further to a minimum value

318   the global entropy generation rate is decreased also to minimum value and not

319   equal to zero. From figure 7 and 8, at maximum Reynolds number, the

320   NACA0012 give lower entropy generation rate than other airfoil. From figure 9, it

321   is concluded that the NACA0015 give lower maximum value for the global

322   entropy generation rate than other airfoil in both cycles. The NACA0015 airfoil

323   section gives less average value ranging from 20% less to 10% of the global

324   entropy generation rate during the sinusoidal wave cycle see figure 10. To confirm

325   these results we have made a comparison between the second law efficiency for

326   four different airfoils at compression and suction cycle (figure 11) and also for the

327   total average efficiency during the sinusoidal wave cycle (figure 12), NACA0015

328   gives best efficiency when it is compared with other airfoils in both compression

329   and suction cycle and therefore in total sinusoidal wave cycle ranging from 2%

330   less to 1%. In four different airfoils and at certain angle of attack, the efficiency

331   for compression cycle higher than suction cycle ranging from 1% less to 0.3%.

332   Equation (17) is defining the exergy value, which can be written as:

333      $$Exergy = KE + S_G \qquad\qquad\qquad (17)$$

334   Contours of Exergy around the blade of NACA0015 for angle of attack 2 degree at

335 different time and different velocity along the sinusoidal wave can be seen in figure (13)

336 that the positive value of velocity refers to compression cycle and the negative value

337 refers to suction cycle. From this figure it can be observed that as the velocity increase

338 the value of exergy around the blade increase, otherwise, the leading and trailing edge

339 always have the lowest value, but at compression cycle the area around the trailing edge

340 has lower value than the leading edge, and in the suction cycle the area around the

341 leading edge has lower value than trailing one.

342

343 **3.2 Effect of the angle of attack on entropy generation**

344 The increase of angle of attack has a direct effect to the entropy generation in
345 the flow over the airfoil which is similar to the effect of Reynolds number.
346 However, as shown in figure 14(a) and (b), NACA0015 airfoil has a different
347 entropy generation signature for different angles of attack listed in table 2. For
348 accelerating flow in compression cycle, Figure 14 (a) at Reynolds number equal to
349 1.2×10^5 the maximum value of global entropy generation rate occurs due to 2
350 degree angle of attack but the minimum value of it occurs due to -15 degree angle
351 of attack. The 17 degree angle of attack gives maximum global entropy generation
352 rate at 1.7×10^5 Reynolds number, and the minimum value occurs due to -11
353 degree at the same Reynolds number. Finally, at Reynolds number equal to
354 2.3×10^5 and 2.4×10^5 the maximum global entropy generation rate occurs due to 17
355 degree and the minimum value occurs due to 5 degree.

356

357 The trend of global entropy generation rate at suction cycle is different
358 from the compression cycle at various angles which can be seen in figure 14 (b).
359 For decelerating flow in suction cycle at Reynolds number equal to 1.7×10^5, the
360 maximum global entropy generation rate occurs at 5 degree angle of attack and the
361 minimum value occurs due to 25 degree. For Reynolds number equal to 1.2×10^5
362 the maximum global entropy generation rate occurs due to 2 degree angle of attack
363 and the minimum value due to 25 degree. Low angles of attack around zero, both
364 positive and negative direction have higher global entropy generation rate and
365 lower entropy efficiency except at 17 degree so we can note that there is
366 unexpected increase in the value of global entropy generation rate accompanied by
367 a lack of the second law efficiency, see figure 15 and 16. As For angle of attack
368 from -5 to 5 degree the entropy efficiency for compression cycle higher than the
369 suction cycle ,but when the angle of attack increase in both directions the
370 efficiency for suction cycle exceeds the compression cycle, see figure 17. At same
371 angle of attack but in different direction, the positive direction gives higher
372 efficiency than the negative one. For example, the second law efficiency for 5
373 degree higher approximately 0.5% than -5 degree and approximately 0.1%
374 between 11 and -11 degree and finally 0.3% between 15 and -15 degree.

4. CONCLUSIONS

Second law analysis of Wells turbine requires accurate estimation of flow irreversibilities around the turbine blades. Two-dimensional incompressible unsteady flow simulations of different airfoils reveals that the geometry and the operating conditions have radical effects on the global entropy generation rate in the flow around turbine airfoil. The main conclusions are summarized as follows.

1- The relationship between the Reynolds number and the global entropy generation rate haven't a direct correlation but when compare between four airfoils at certain angle of attack the maximum global entropy generation rate occurs at Reynolds number of 1.2×10^5 and at 1.7×10^5 (2×10^5 for NACA0012 in compression cycle) less than halved.

2- NACA0015 gives less global entropy generation rate and higher efficiency compare with other airfoil.

3- The efficiency for four different airfoils in compression cycle is higher than suction cycle at 2 degree angle of attack. But when the angle of attack increase, the efficiency for suction cycle increase also more than the compression one.

4- At zero and low angle of attack we have higher global entropy generation rate than at high angle of attack.

5- From the study of the behavior of four different airfoils, NACA0015 isn't the best airfoil in all condition .For examples, at maximum Reynolds number NACA0012 gives less global entropy generation rate and NACA0020 create the minimum value, so it is a good concept to create an optimum design airfoil gives better result than NACA0015.

6- In general the global entropy generation rate due to viscous dissipation is a very sensitive indicator for airfoils behavior at any change in design parameters, the operating condition and also being affected by flow direction.

5. Acknowledgements

Department of marine Engineering at Arab Academy for Science, Technology and Maritime Transport.

6.   REFERENCES

[1] T.J.T.e.a. Whittaker, The Queen's university of Belfast Axisymmetric and Multi-resonant Wave Energy Converters, Trans. ASME. J. Energy Resources Tech., 107 (1985) pp. 74-80.

[2] T.J.T.a.M. Whittaker, F. A. , Design Optimisation of Axisymmetric Tail Tube Buoys, in: IUTAM, Symposium on Hydrodynamics of Ocean Wave Energy Conversion, Lisbon,July., 1985.

[3] T.J.J. Whittaker, McIlwain, S. T. and Raghunathan, S. , Islay Shore Line Wave Power Station, Proceedings European Wave Energy Symposium., Paper G6, Edinburgh. (1993).

[4] S. Raghunathan, Theory and Performance of Wells Turbine, Queen's University of Belfast, Rept. WE/80/13R (1980).

[5] M.M. Rashidi, M. Ali, N. Freidoonimehr, F. Nazari, Parametric Analysis and Optimization of Entropy Generation in Unsteady MHD Flow over a Stretching Rotating Disk Using Artificial Neural Network and Particle Swarm Optimization Algorithm, Energy, 55 (2013) 497-510.

[6] S.C. Kaushik, V.S. Reddy, S.K. Tyagi, Energy and Exergy Analyses of Thermal Power Plants: A Review, Renewable and Sustainable Energy Reviews, 15 (2011) 1857-1872.

[7] A. Bejan, Entropy Generation Minimization: The Method of Thermodynamic Optimization of Finite-Size Systems and Finite-Time Processes, Taylor & Francis, (1995).

[8] A. Bejan, Entropy Generation Minimization- The New Thermodynamics of Finite-Size Devices and Finite-Time Processes, Applied Physics Reviews, (1996).

[9] L.M.C. Gato, R. Curran, The Energy Conversion Performance of Several Types of Wells Turbine Designs, Proceedings of the Institution of Mechanical Engineers, Part A: Journal of Power and Energy, 211 (1997) 133-145.

[10] T. Setoguchi, Effect of Guide Vane Shape on the Performance of a Wells Turbine, Renewable Energy, 23 (2001) 1-15.

[11] M. Takao, T. Setoguchi, T.H. Kim, K. Kaneko, M. Inoue, The Performance of a Wells Turbine with 3D Guide Vanes, International Journal of Offshore and Polar Engineering, 11 (2001) 72-76.

[12] M. Mamun, Y. Kinoue, T. Setoguchi, K. Kaneko, A.K.M.S. Islam, Improvement af the Performance of the Wells Turbine by using a Very Thin Elongated Endplate at the Blade Tip, in: the 3rd BSME-ASME International Conference on Thermal Engineering, ASME, Dhaka, Bangladesh, 2006.

[13] M. Takao, T. Setoguchi, Y. Kinoue, K. Kaneko, Wells Turbine with End Plates for Wave Energy Conversion, Ocean Engineering, 34 (2007) 1790-1795.

[14] A. Thakker, P. Frawley, E.S. Bajeet, Numerical Analysis of Wells Turbine Performance Using a 3D Navier Stokes Explicit Solver, in: International Offshore and Polar Engineerbtg Conference, Stavanger, Norway, 2001.

451 [15] Tae-Hun Kim, Yeon- Won Lee, Ill-Kyoo Park, Toshiaki Setoguchi, C.-S. Kang,
452 Numerical Analysis for Unsteady Flow Characteristics of the Wells Turbine, in:
453 International Offshore and Polar Engineering Conference, The International Society of
454 Offshore and Polar Engineers, Kitakyushu, Japan, 2002, pp. 694-699.
455 [16] T. Setoguchi, M. Takao, K. Itakura, M. Mohammad, K. Kaneko, A. Thakker,
456 Effect of Rotor Geometry on the Performance of Wells Turbine, in: The Thirteenth
457 International Offshore and Polar Engineering Conference, The International Society of
458 Offshore and Polar Engineers, Honolulu, Hawaii, USA, 2003, pp. 374-381.
459 [17] T.S. Dhanasekaran, M. Govardhan, Computational Analysis of Performance and
460 Flow Investigation on Wells Turbine for Wave Energy Conversion, Renewable Energy,
461 30 (2005) 2129-2147.
462 [18] M.H. Mohamed, G. Janiga, D. Th´evenin, Performance Optimization of a Modified
463 Wells Turbine using Non-Symmetric Airfoil Blades, in: Turbo Expo 2008: Power for
464 Land, Sea and Air GT, ASME, Berlin, Germany, 2008.
465 [19] M.H. Mohamed, Design Optimization of Savonius and Wells Turbines, in,
466 University of Magdeburg,Germany, Germany, 2011.
467 [20] Y. Kinoue, T.H. Kim, T. Setoguchi, M. Mohammad, K. Kaneko, M. Inoue,
468 Hysteretic Characteristics of Monoplane and Biplane Wells Turbine for Wave Power
469 Conversion, Energy Conversion and Management, 45 (2004) 1617-1629.
470 [21] M. Mamun, Y. Kinoue, T. Setoguchi, T.H. Kim, K. Kaneko, M. Inoue, Hysteretic
471 Flow Characteristics of Biplane Wells Turbine, Ocean Engineering, 31 (2004) 1423-
472 1435.
473 [22] T. Setoguchi, Y. Kinoue, T.H. Kim, K. Kaneko, M. Inoue, Hysteretic
474 Characteristics of Wells Turbine for Wave Power Conversion, Renewable Energy, 28
475 (2003) 2113-2127.
476 [23] T.H. Kim, T. Setoguchi, Y. Kinoue, K. Kaneko, M. Inoue, Hysteretic
477 Characteristics of Wells Turbine for Wave Power Conversion, in: The Twelfth
478 International Offshore and Polar Engineering Conference, The International Society of
479 Offshore and Polar Engineers, Kitakyushu, Japan, 2002, pp. 687-693.
480 [24] T.M. Setoguchi T, Kaneko K., Hysteresis on Wells Turbine Characteristics in
481 Reciprocating Flow, International Journal of Rotating Machinery, 4 (1998) 17-24.
482 [25] Y. Kinoue, T. Setoguchi, T.H. Kim, K. Kaneko, M. Inoue, Mechanism of
483 Hysteretic Characteristics of Wells Turbine for Wave Power Conversion, Journal of
484 Fluids Engineering, 125 (2003) 302.
485 [26] M. Mamun, The Study on the Hysteretic Characteristics of the Wells Turbine in a
486 Deep Stall Condition, in: Energy and Material Science Graduate School of Science and
487 Engineering, Saga University, Japan, 2006, pp. 141.
488 [27] S. Shaaban, Insight Analysis of Biplane Wells Turbine Performance, Energy
489 Conversion and Management, 59 (2012) 50-57.
490 [28] L.M.C. Gato, R. Curran, Performance of the Contrarotating Wells Turbine,
491 International Journal of Offshore and Polar Engineering, 6 (1996) 68-75.
492 [29] M. Folley, R. Curran, T. Whittaker, Comparison of LIMPET Contra-rotating Wells
493 Turbine with Theoretical and Model Test Predictions, Ocean Engineering, 33 (2006)
494 1056-1069.
495 [30] Y. Kinoue, T. Setoguchi, T. Kuroda, K. Kaneko, M. Takao, A. Thakker,
496 Comparison of Performances of Turbines for Wave Energy Conversion, Journal of
497 Thermal Science, 12 (2003) 323-328.

498 [31] M. Takao, A. Thakker, R. Abdulhadi, T. Setoguchi, Effect of Blade Profile on the
499 Performance of a Large-scale Wells Turbine for Wave-energy Conversion, International
500 Journal of Sustainable Energy, 25 (2006) 53-61.
501 [32] A. Thakker, R. Abdulhadi, Effect of Blade Profile on the Performance of Wells
502 Turbine under Unidirectional Sinusoidal and Real Sea Flow Conditions, International
503 Journal of Rotating Machinery, 2007 (2007) 1-9.
504 [33] A. Thakker, R. Abdulhadi, The Performance of Wells Turbine Under Bi-
505 Directional Airflow, Renewable Energy, 33 (2008) 2467-2474.
506 [34] K. Pope, I. Dincer, G.F. Naterer, Energy and Exergy Efficiency Comparison of
507 Horizontal and Vertical Axis Wind Turbines, Renewable Energy, 35 (2010) 2102-2113.
508 [35] O. Baskut, O. Ozgener, L. Ozgener, Effects of Meteorological Variables on
509 Exergetic Efficiency of Wind Turbine Power Plants, Renewable and Sustainable Energy
510 Reviews, 14 (2010) 3237-3241.
511 [36] A.M. Redha, I. Dincer, M. Gadalla, Thermodynamic Performance Assessment of
512 Wind Energy Systems: An Application, Energy, 36 (2011) 4002-4010.
513 [37] O. Ozgener, L. Ozgener, Exergy and Reliability Analysis of Wind Turbine
514 Systems: A Case Study, Renewable and Sustainable Energy Reviews, 11 (2007) 1811-
515 1826.
516 [38] O. Baskut, O. Ozgener, L. Ozgener, Second Law Analysis of Wind Turbine Power
517 Plants: Cesme, Izmir Example, Energy, 36 (2011) 2535-2542.
518 [39] C.L. Iandoli, 3-D Numerical Calculation of the Local Entropy Generation Rates in
519 a Radial Compressor Stage, International journal of thermodynamics, 8 (2005) 83-94.
520 [40] E.M. Wahba, A Computational Study of Viscous Dissipation and Entropy
521 Generation in Unsteady Pipe Flow, Acta Mechanica, 216 (2010) 75-86.
522 [41] S.D. Launder Be, The Numerical Computation of Turbulent Flows, Computer
523 Methods in Applied Mechanics and Engineering, 3 (1974) 269-289.
524 [42] D.C. Wilcox, Turbulence Modeling for Computational Fluid Dynamics, DCW
525 Industries, Incorporated, 2006.
526 [43] C. Hirsch, Numerical Computation of Internal and External Flows: The
527 Fundamentals of Computational Fluid Dynamics, Elsevier Science, 2007.
528 [44] R. Starzmann, T. Carolus, Model-Based Selection of Full-Scale Wells Turbines for
529 Ocean Wave Energy Conversion and Prediction of their Aerodynamic and Acoustic
530 Performances, Proceedings of the Institution of Mechanical Engineers, Part A: Journal
531 of Power and Energy, 228 (2013) 2-16.
532 [45] M.H. Mohamed, S. Shaaban, Optimization of Blade Pitch Angle of an Axial
533 Turbine Used for Wave Energy Conversion, Energy, 56 (2013) 229-239.
534 [46] M. Torresi, S.M. Camporeale, G. Pascazio, Detailed CFD Analysis of the Steady
535 Flow in a Wells Turbine Under Incipient and Deep Stall Conditions, Journal of Fluids
536 Engineering, 131 (2009) 071103.
537 [47] C.A.K. DE Moura, Carlos S., The Courant–Friedrichs–Lewy (CFL) Condition: 80
538 Years After Its Discovery, 1 ed., Birkhäuser Basel, Boston, 2013.
539 [48] M.H. Mohamed, S. Shaaban, Numerical Optimization of Axial Turbine with Self-
540 pitch-controlled Blades used for Wave Energy Conversion, International Journal of
541 Energy Research, (2013) n/a-n/a.
542 [49] M.H. Mohamed, G. Janiga, E. Pap, D. Thévenin, Multi-objective Optimization of
543 the Airfoil Shape of Wells Turbine used for Wave Energy Conversion, Energy, 36
544 (2011) 438-446.

545   [50] R.E. Sheldahl, P.C. Klimas, Aerodynamic Characteristics of Seven Symmetrical
546   Airfoil Sections Through 180-Degree Angle of Attack for Use in Aerodynamic Analysis
547   of Vertical Axis Wind Turbines, in: Sandia National Laboratories energy report, the
548   United States of America, 1981, pp. 118.
549   [51] T. Nomura, Y. Suzuki, M. Uemura, N. Kobayashi, Aerodynamic Forces on a
550   Square Cylinder in Oscillating Flow with Mean Velocity, Journal of Wind Engineering
551   and Industrial Aerodynamics, 91 (2003) 199–208.
552   [52] A.S. Shehata, K.M. Saqr, M. Shehadeh, Q. Xiao, A.H. Day, Entropy Generation
553   Due to Viscous Dissipation around a Wells Turbine Blade: A Preliminary Numerical
554   Study, Energy Procedia, 50 (2014) 808-816.
555   [53] T.M. A. Okajima, S. Kimura,, Force Measurements and Flow Visualization of
556   Circular and Square Cylinders in Oscillatory Flow, Proc. JSME B 63 (615), (1997) 58–
557   66.
558   [54] R.D. Blevins, Flow-Induced Vibration, 2nd Edition ed., Van Nostrand Reinhold,
559   New York, 1990.

560
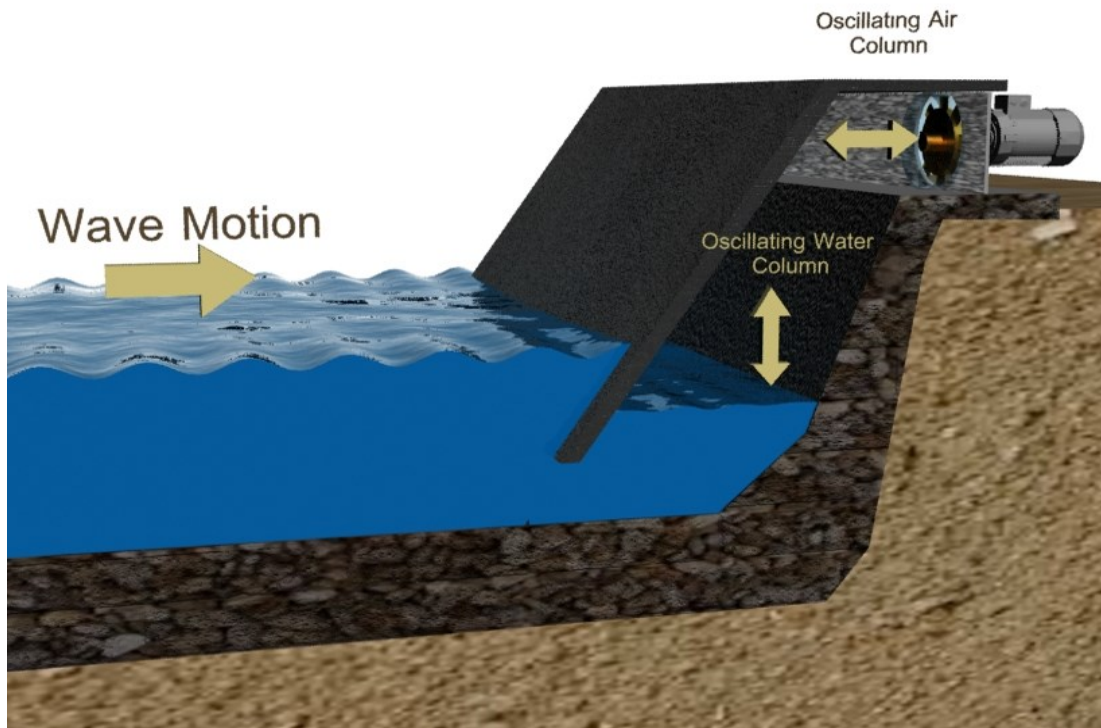
Figure 1.a. An illustration of the principle of operation of OWC system, where the wave motion is used to drive a turbine through the oscillation of air column.
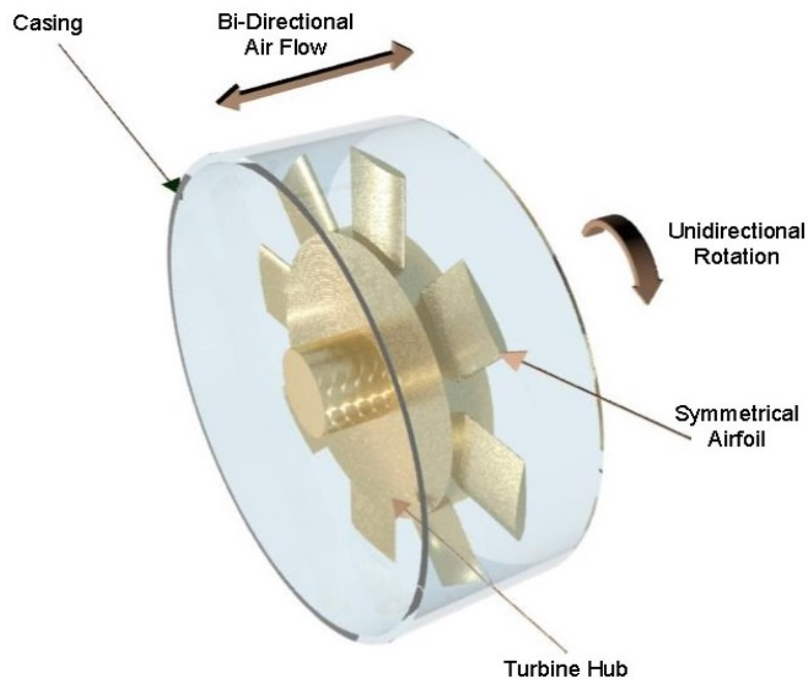
Figure 1.b. Typical structure of W-T rotor.
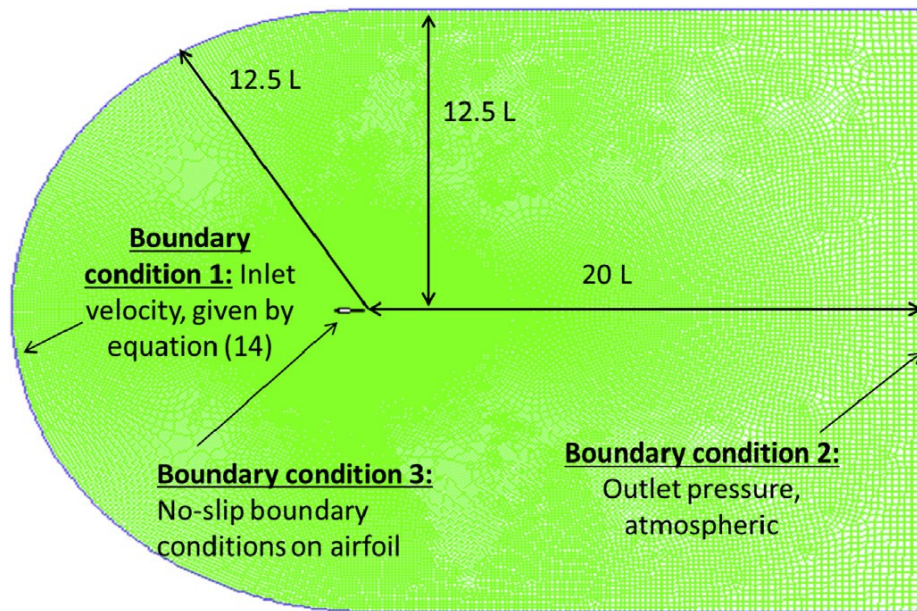
Figure (2) the dimensions of whole computational domain and location of airfoil
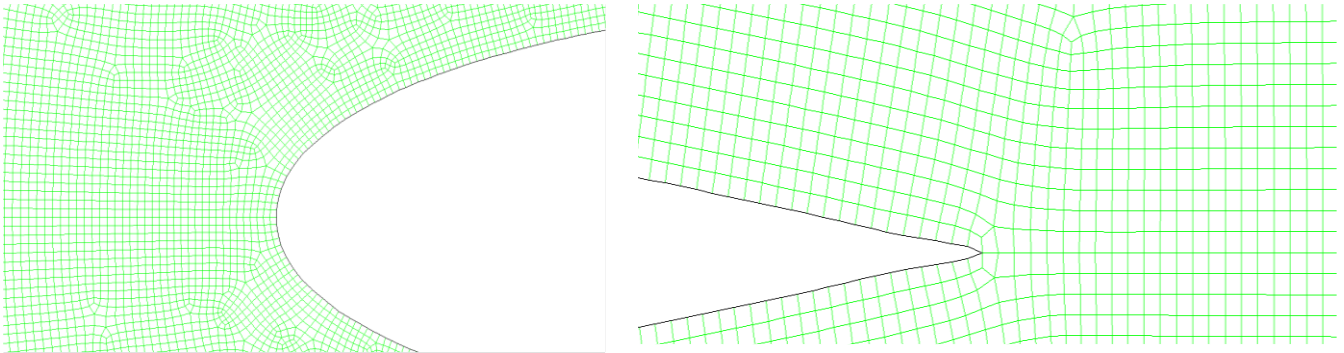
Figure 3. Computational grid near the wall of the airfoil
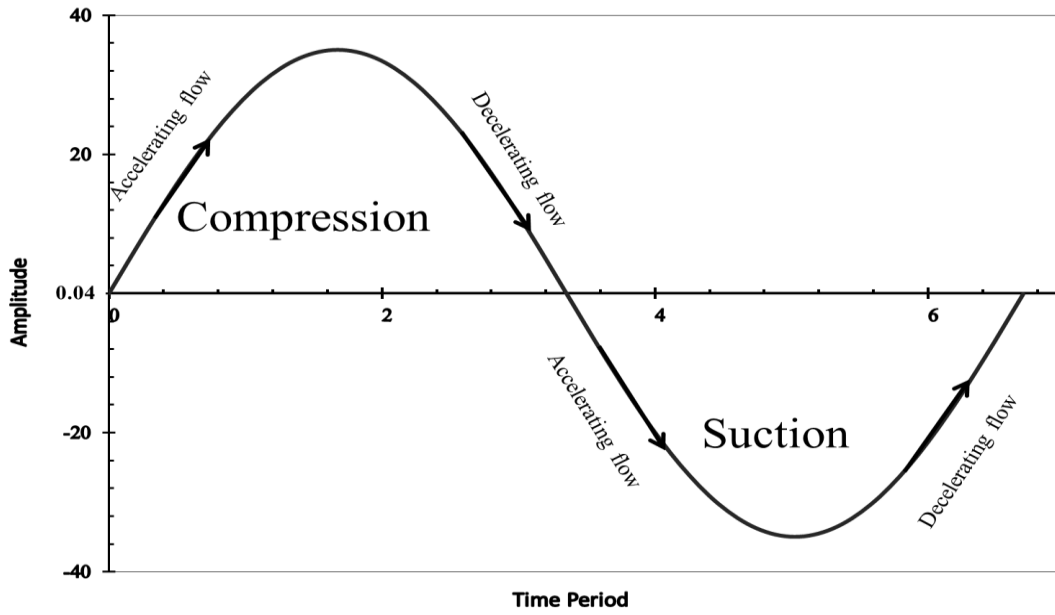
Figure 4.The sinusoidal wave boundary condition, which represent a regular oscillating water column
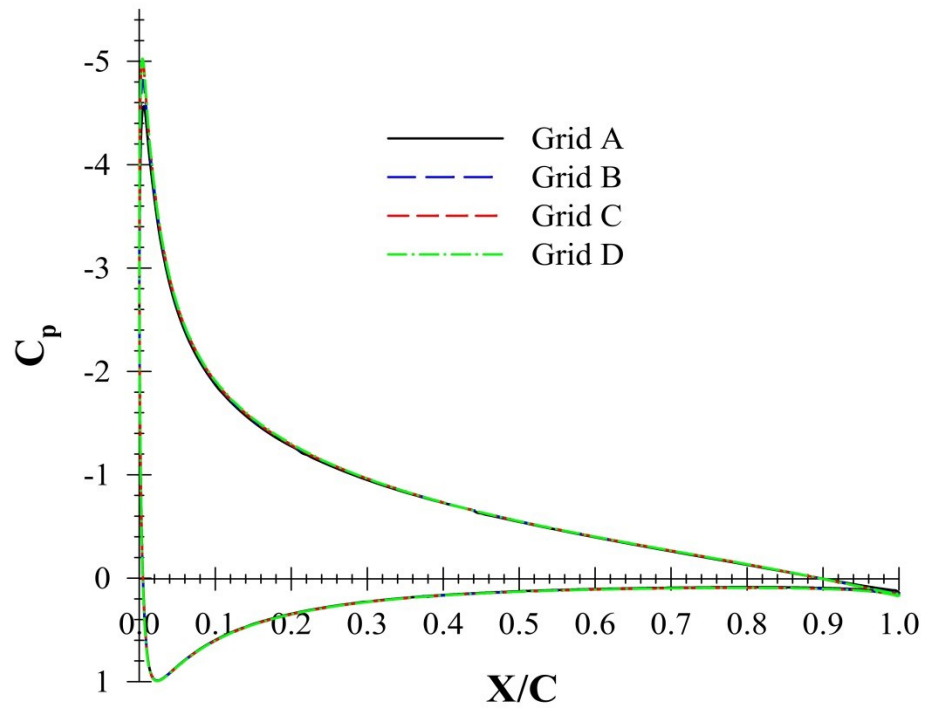
Figure 5. Pressure coefficient plotted on the normalized airfoil cord for different grid resolutions.
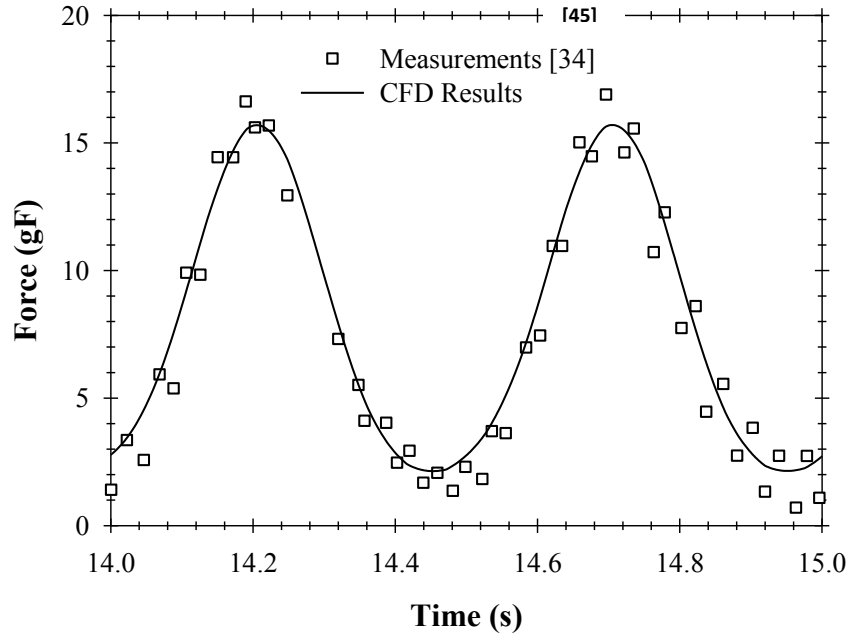
Figure 6(a) Measured unsteady in-line force F_D **(angle of attack= 0 degree) and** F_D **calculated from CFD for frequency 2 Hz**.
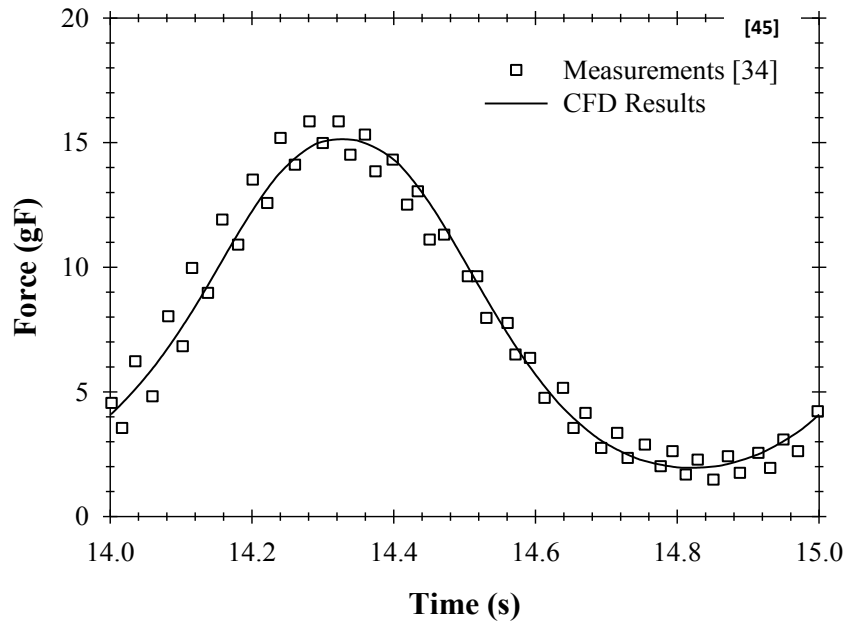
Figure 6(b) Measured unsteady in-line force F_D **(angle of attack= 0 degree) and** F_D **calculated from CFD for frequency 1 Hz.**

23
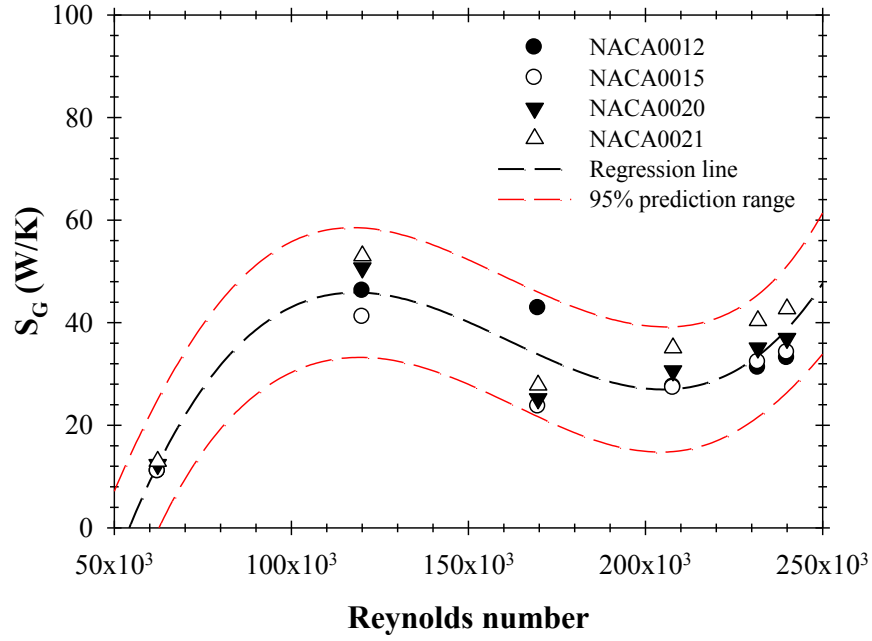
Figure 7(a) the global entropy generation rate variation with different Reynolds's number at accelerating flow in compression cycle for four different airfoils
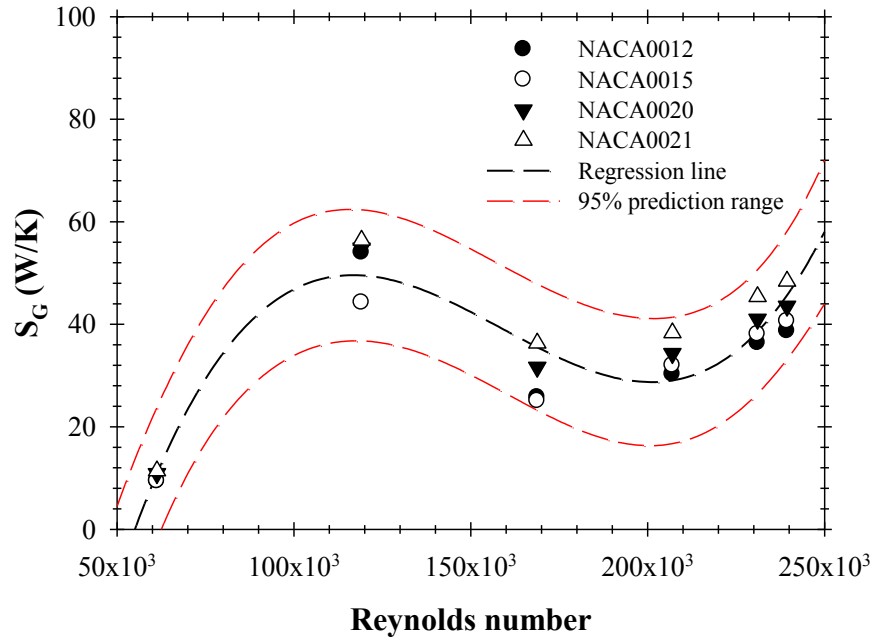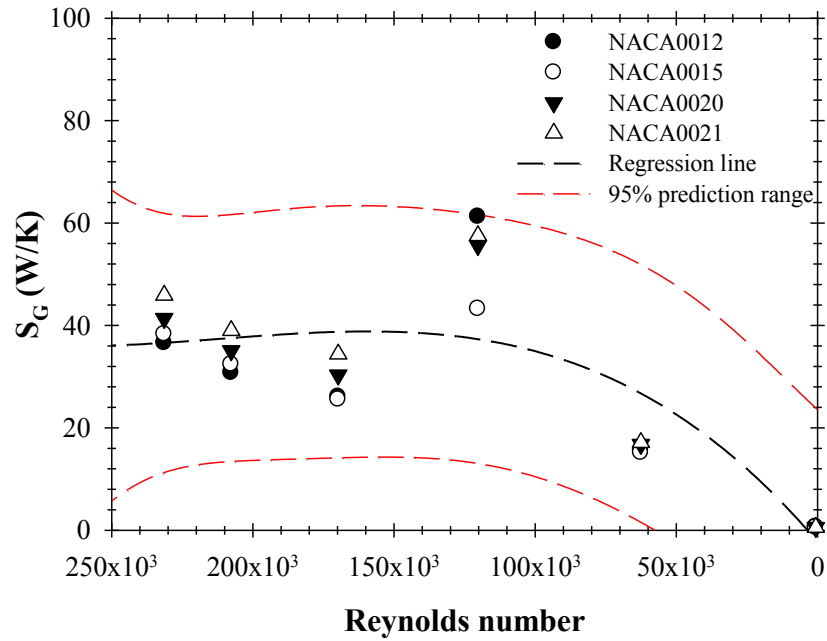

Figure 7(b) the global entropy generation rate variation with different Reynolds's number at accelerating flow in suction cycle for four different airfoils
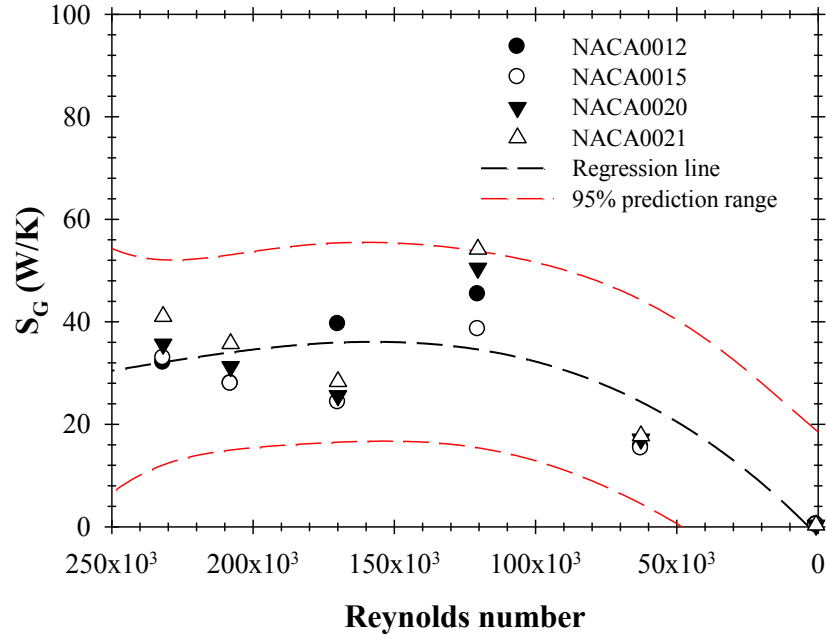
Figure 8(a) the global entropy generation rate variation with different Reynolds's number at decelerating flow in compression cycle for four different airfoils

Figure 8(b) the global entropy generation rate with different Reynolds's number at decelerating flow in suction cycle for four different airfoils
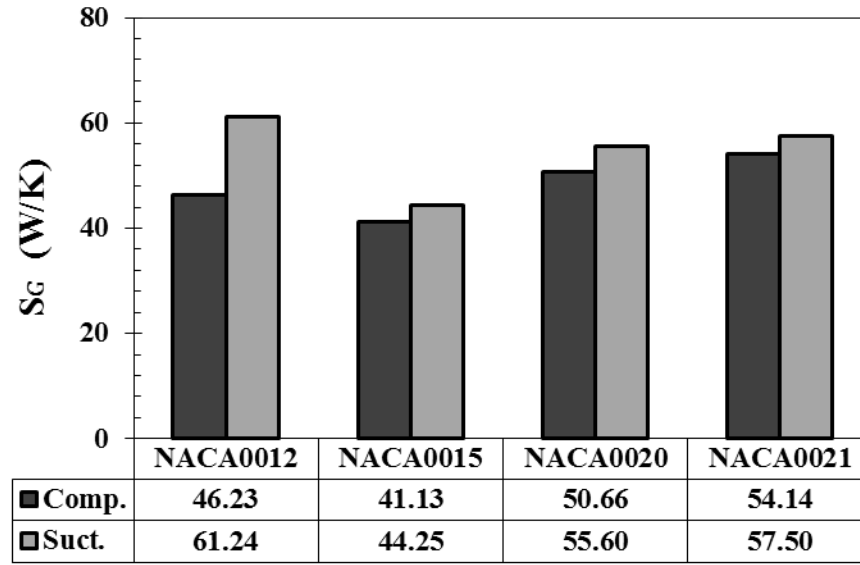
	NACA0012	NACA0015	NACA0020	NACA0021
■Comp.	46.23	41.13	50.66	54.14
▨Suct.	61.24	44.25	55.60	57.50

Figure 9 The maximum value for the global entropy generation rate at compression and suction cycle

	NACA0012	NACA0015	NACA0020	NACA0021
■Average value	30.078	27.341	31.373	34.321
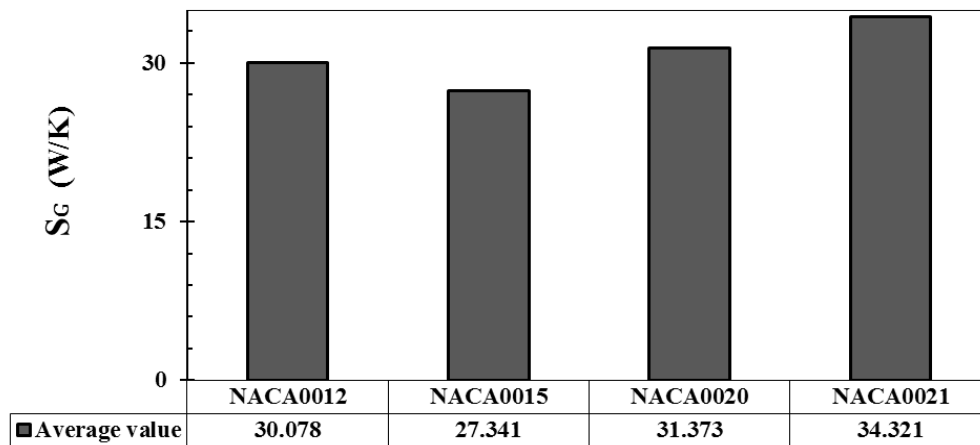
Figure 10 Comparisons between the global entropy generation rate during the sinusoidal wave cycle for four different airfoils

	NACA0012	NACA0015	NACA0020	NACA0021
■ Comp.	79.71%	80.89%	79.60%	78.82%
□ Suction	79.46%	80.28%	78.75%	78.07%
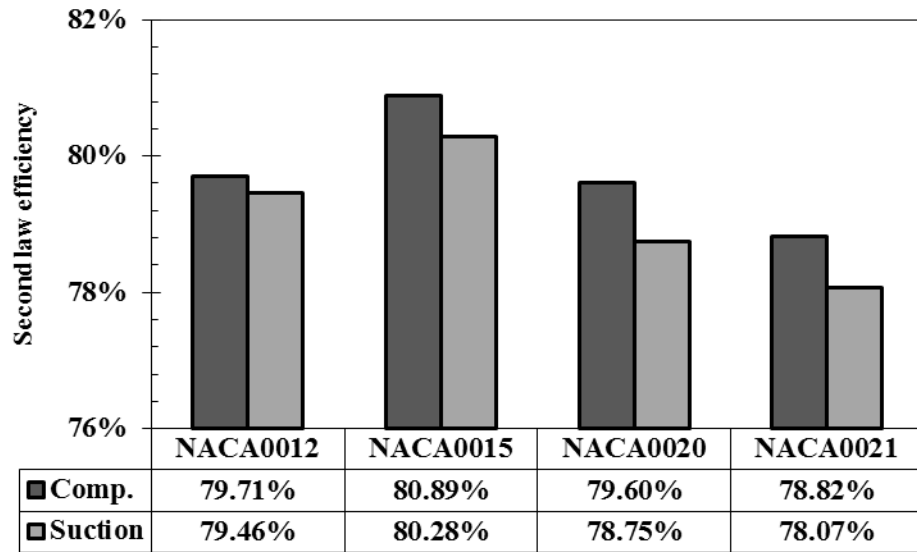
Figure 11 Comparisons between second law efficiency during the compression and suction wave cycle for four different airfoils

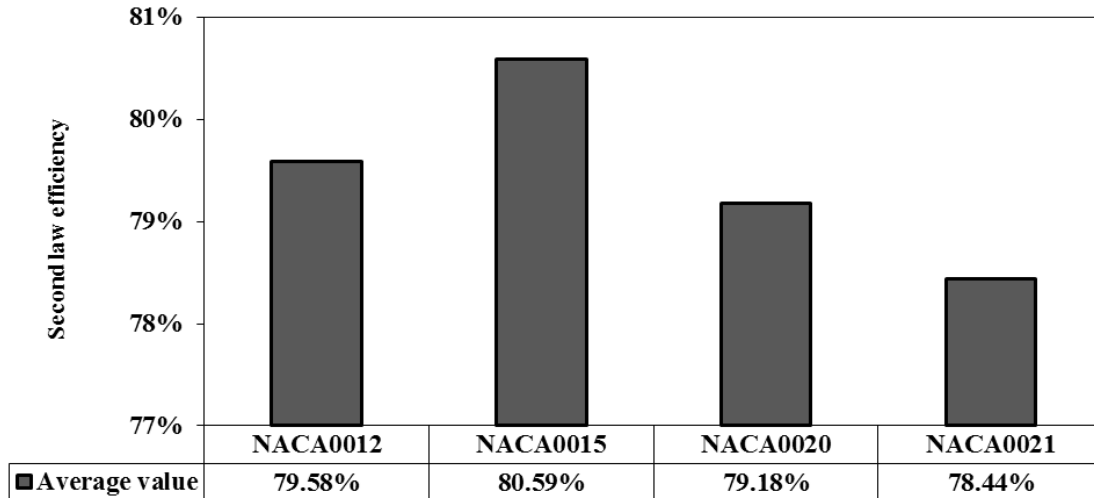|	NACA0012	NACA0015	NACA0020	NACA0021
■ Average value	79.58%	80.59%	79.18%	78.44%

Figure 12 Comparisons between second law efficiency during the sinusoidal wave cycle for four different airfoils
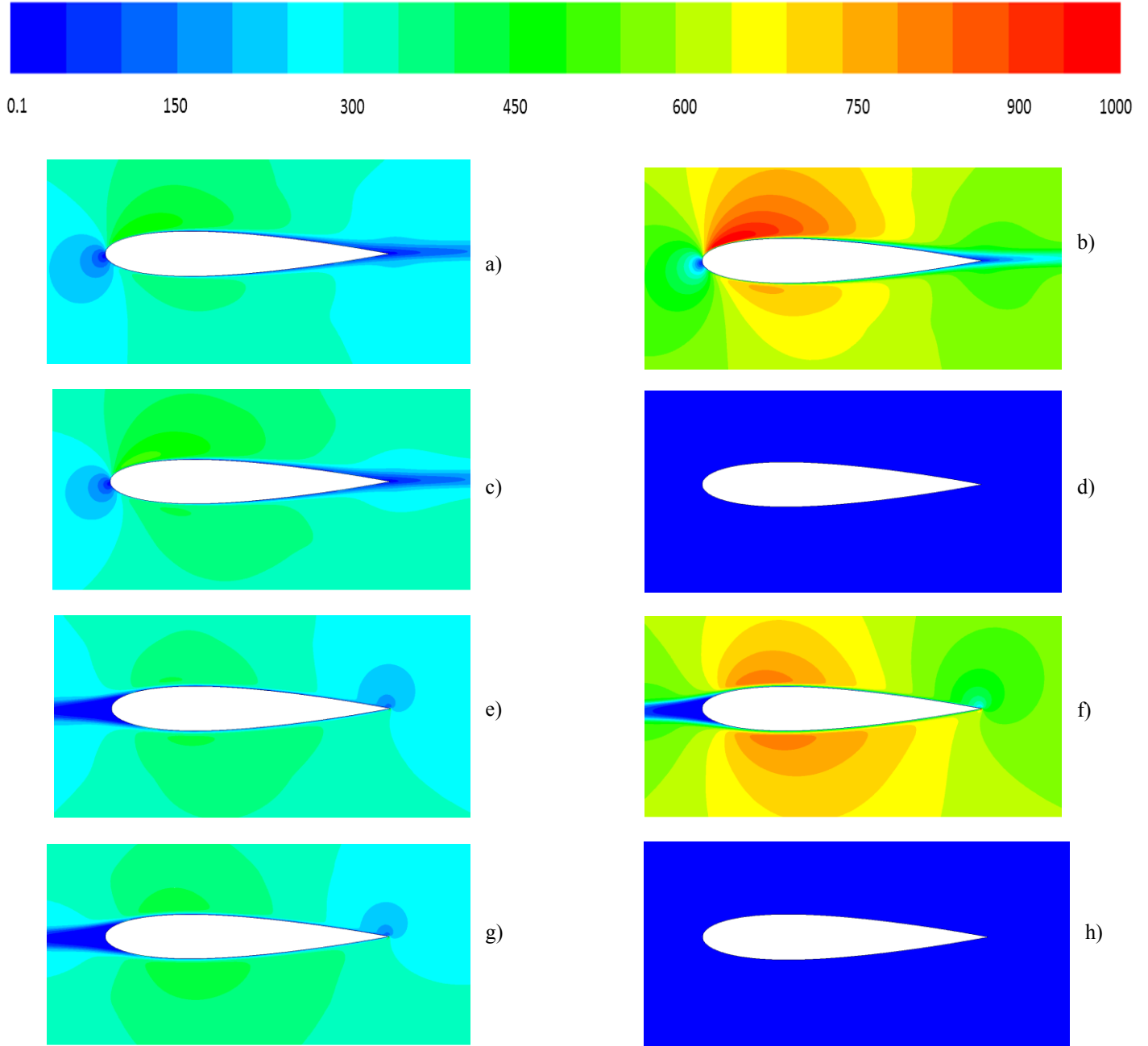
Figure 13. Contours of Exergy around the blade of NACA0015 for angle of attack 2 degree at different time and different velocity along the sinusoidal wave, a) at t =0.837 s and V =24.778 m/s, b) t = 1.674 s and V =35.04 m/s, c) t =2.511 s and V =24.824 m/s, d) t =3.348 s and V =0.10565 m/s, e) t =4.185 s and V =-24.7 m/s, f) t =5.022 s V =-35 m/s, g) t =5.859 s and V =-24.79 m/s, h) t =6.696 s and V =-0.0913 m/s.
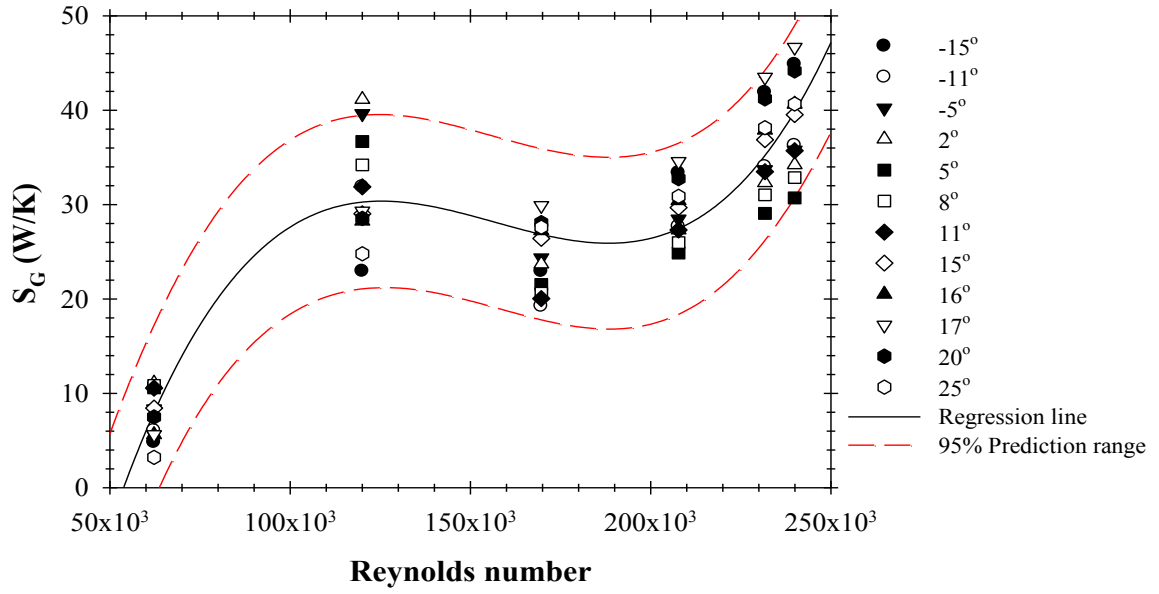
Figure 14 (a) the global entropy generation rate variation with different Reynolds's at accelerating flow in compression cycle for NACA0015 airfoil with different angle of attack.
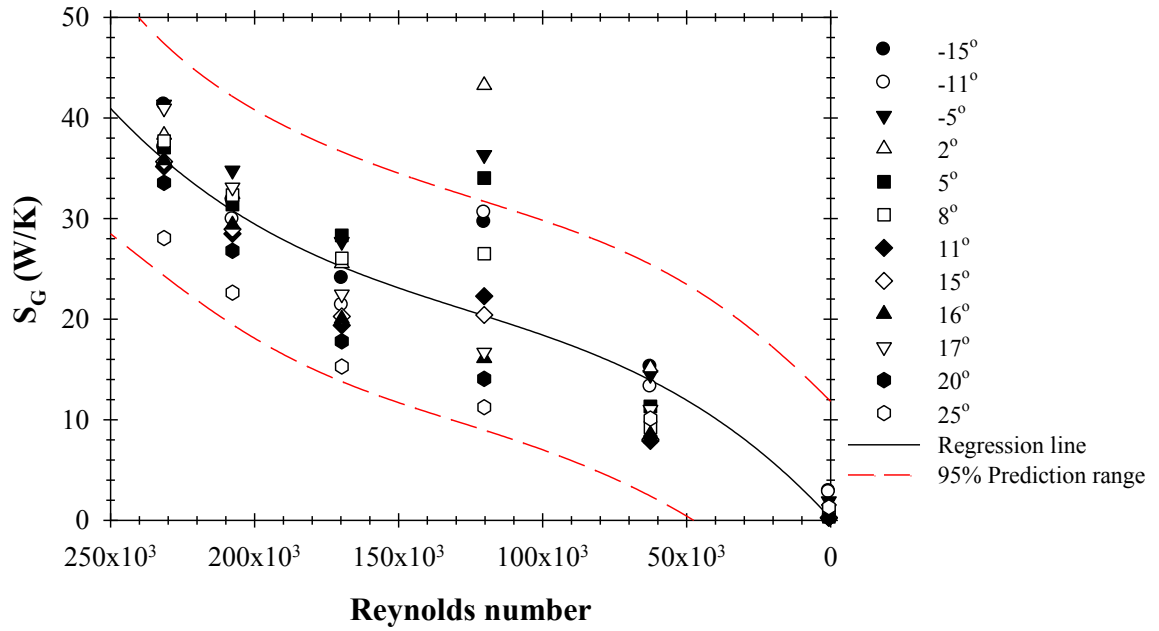

Figure 14 (b) the global entropy generation rate variations with different Reynolds's at decelerating flow in suction cycle for NACA0015 airfoil with different angle of attack.
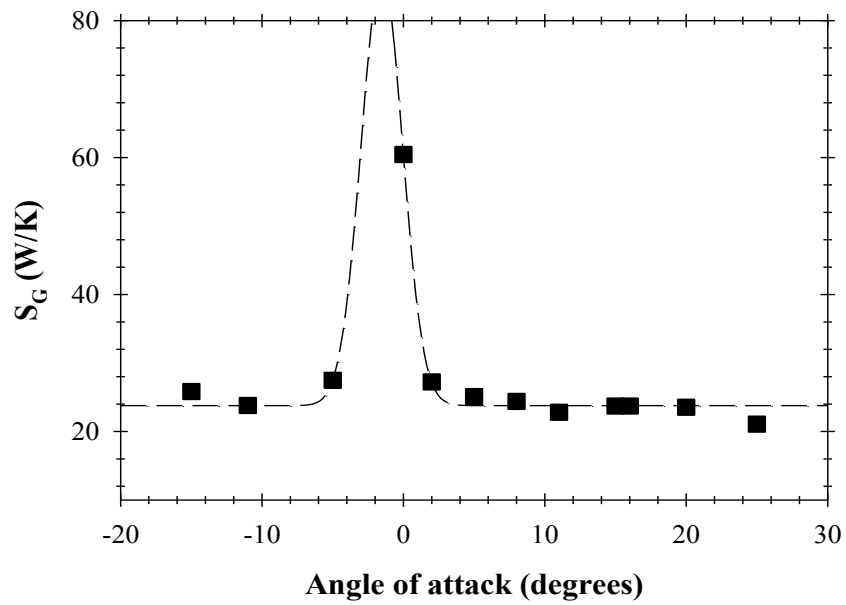
Figure 15 the global entropy generation rate during the sinusoidal wave cycle for different angle of attack. The dotted line indicates a fitting with a Gaussian distribution function.
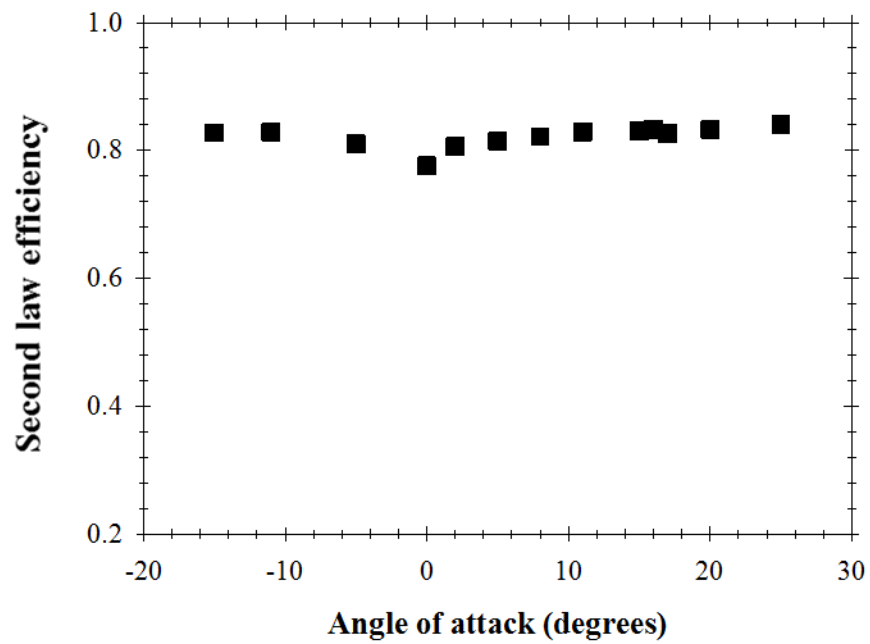

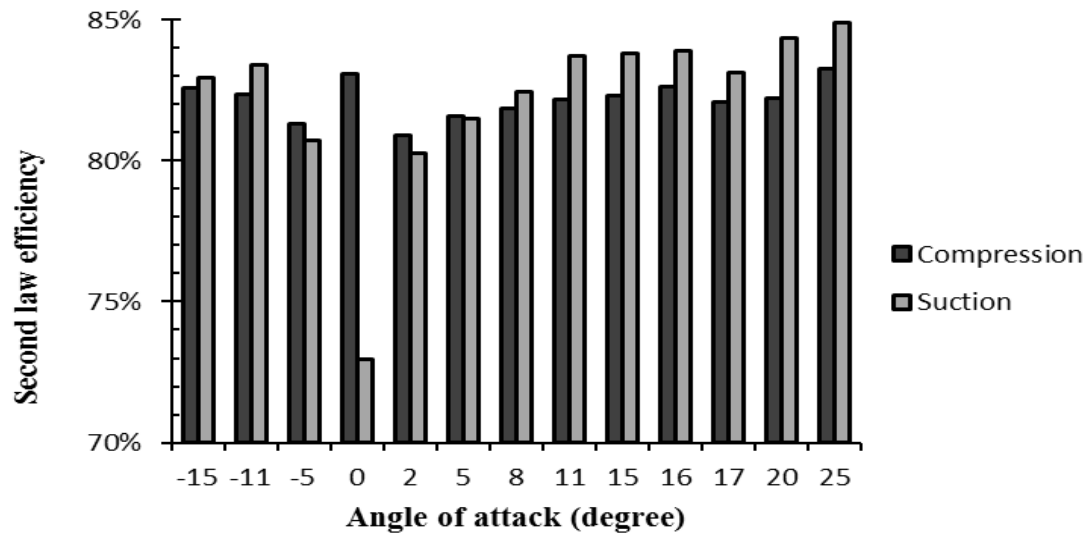**Figure 16 Second low efficiency during the sinusoidal wave cycle for different angle of attack**

Figure 17 Comparisons between second law efficiency during the compression and suction wave cycle for different angle of attack

Table 1 Specification of different grids used in the grid independence test

Grid	No. of Cells	first cell	Growth rate	Aspect ratio	EquiAngle skew
A	112603	1×10^{-4}	1.02	1.996	0.429
B	200017	1×10^{-5}	1.015	2.466	0.475
C	312951	1×10^{-5}	1.012	2.376	0.514
D	446889	1×10^{-6}	1.01	2.551	0.513

Table 2 the direction for positive and negative value of angle of attack.

Angle of attack	x component of velocity direction	y component of velocity direction
-15	0.965926	-0.258819
-11	0.981627	-0.190809
-5	0.996195	-0.087156
0	1	0
2	0.999391	0.0348995
5	0.996195	0.087156
8	0.990268	0.139173
11	0.981627	0.190809
15	0.965926	0.258819
16	0.961262	0.275637
17	0.956305	0.292372
20	0.939693	0.342020
25	0.906308	0.422618